



A 400-year reconstruction of wintertime Arctic sea-ice extent using a high-elevation, mid-latitude tree-ring record

P. T. Soulé¹ · P. A. Knapp²

Received: 3 October 2018 / Revised: 10 April 2019 / Accepted: 30 May 2019 / Published online: 17 June 2019
© ISB 2019

Abstract

We examined relationships between wintertime Arctic sea-ice extent (ASIE) and radial growth rates of alpine larch trees (LALY) in the northern Rockies, USA, during 1979–2015 ($r = -0.71$, $p < 0.01$) and reconstructed ASIE fluctuations from 1613 to 2015. Wintertime ASIE corresponds with summertime mid-latitude upper-level atmospheric flow patterns with ridging (troughing) and warmer (cooler) conditions prevailing in the Rockies when ASIE are below (above) average. In turn, warmer (cooler) summertime conditions favor (disfavor) growth of LALY, thus “recording” interannual variations in ASIE. Both 1000 hPa temperatures and 500 hPa geopotential heights during years of anomalously high or low radial growth negatively correspond with ASIE, suggesting that a disjunct spatial influence on atmospheric conditions may be associated with interannual variability of ASIE. Reconstructed ASIE values show that 1996–2015 was the lowest 20-year period on record, but the mean value is not significantly different from six other distinct periods of below-average ASIE.

Keywords Arctic sea-ice extent · Reconstruction · Tree-rings · Alpine larch · 500 hPa flow · Montana · USA

Introduction

Declining Arctic sea-ice extent (ASIE) is implicated in changes in mid-latitude weather (Cohen et al. 2014; Francis 2017; Screen 2017), although both the mechanisms causing this and the spatiotemporal patterns remain unclear (Overland et al. 2015). Here, we show that changes in wintertime ASIE correspond with summertime upper-level flow in western North America that in turn impact radial growth patterns of alpine larch trees (*Larix lyallii* Parl; LALY). Lower (higher) wintertime ASIE conditions correspond with and possibly cause warmer (cooler) summer growing seasons of the temperature-dependent LALY, allowing for a proxy record of ASIE to be inferred from variations in ring

widths. Thus, interannual variability in ring-widths of LALY offers an opportunity to (1) examine fluctuations in ASIE during the past 400 years to place the current period of low ASIE in historical context, and (2) document the broad-ranging geographical effects of declining ASIE.

A summary of the state of the science by Francis (2017) describes how a suite of recent studies have established linkages between declining ASIE and/or Arctic amplification (AA) and climatic perturbations throughout the northern hemisphere. A recurring finding is that reductions in ASIE produce teleconnections leading to enhanced meridionality and persistence of upper-atmospheric flow (e.g., Budikova and Chechi 2016; Francis and Vavrus 2015; Kim et al. 2014; Hall et al. 2017; Screen 2013; Tang et al. 2013, 2014; Wu et al. 2013). Increases in mid-latitude meridionality caused by a decreased poleward temperature gradient may lead to longer periods of locked-phase weather conditions (Francis 2017; Mann et al. 2017; Trouet et al. 2018) associated with climatic extremes. There is less consensus on future changes, as Vavrus et al. (2017) have modeled increased summertime meridionality that is most pronounced over the mid-latitudes (~45 °N), yet others (e.g., Cattiaux et al. 2016) suggest a future decrease in meridionality of the mid-latitude jet stream.

One limitation of assessing changes caused by ASIE fluctuations is the paucity of records prior to satellite monitoring

Electronic supplementary material The online version of this article (<https://doi.org/10.1007/s00484-019-01739-5>) contains supplementary material, which is available to authorized users.

✉ P. T. Soulé
soulept@appstate.edu

¹ Department of Geography and Planning, Appalachian Tree-Ring Laboratory, Appalachian State University, Boone, NC, USA

² Department of Geography, Environment, and Sustainability, Carolina Tree-Ring Science Laboratory, University of North Carolina-Greensboro, Greensboro, NC, USA

that began in the late 1970s. To that end, various proxy measures have been used to reconstruct regional or entire ASIE, including tree-rings (e.g., Fauria et al. 2010; Kinnard et al. 2011; Zhang et al. 2018a), sediments (e.g., Kinnard et al. 2011; Méheust et al. 2016), corals (e.g., Halfar et al. 2013), historical records (e.g., Kinnard et al. 2011; Walsh et al. 2017), and various properties derived from ice cores (e.g., Kinnard et al. 2011; Spolaor et al. 2016; Zhang et al. 2018a), with some reconstructions based on multiple proxies (e.g., Kinnard et al. 2011; Zhang et al. 2018a). Here, we develop a multi-century climatic reconstruction of mean winter (January–March) ASIE extent based on a regional tree-ring chronology developed from the northern Rocky Mountain region of the USA, a region substantively affected by declining ASIE (Knapp and Soulé 2017). We then discuss linkages between surface-temperature anomalies and 500 hPa flow during years of above- and below-average radial growth and explore longer-term driving forces for ASIE variability. To our knowledge, our study is the first to reconstruct ASIE based solely on a regional tree-ring dataset. Additionally, our dataset derived from trees growing in western Montana, USA, is geographically remote from the Arctic region, potentially further documenting the spatial reach of declining ASIE.

Materials and methods

Collection of tree-ring samples

We collected tree-ring data from mature LALY growing at four study sites within western Montana (Fig. 1). LALY is a deciduous conifer that typically grows in harsh environments at high elevations (2400–2800 m for our sites) during a short (~90-day) growing season (Arno and Habeck 1972). LALY are long-lived (up to 1000 years), and radial growth patterns indicate significant summertime temperature sensitivity (e.g., Graumlich and Brubaker 1986; Kipfmüller 2008; Knapp and Soulé 2011); thus, the species tracks interannual fluctuations of summer-warmth conditions.

We used a selective sampling technique to avoid trees with signs of physical damage (e.g., lightning strikes) that might have impacted radial growth patterns and only chose open-canopy trees to avoid growth fluctuations associated with neighboring tree competition and senescence. We obtained two core samples per tree using increment borers and stored the samples in paper straws to air-dry.

Laboratory processing of tree-ring samples

We glued each sample to a supporting mount and sanded multiple times with 200–1000 grit sandpaper until the cellular structure was clear under magnification. We crossdated (Stokes 1996) each sample using the list method

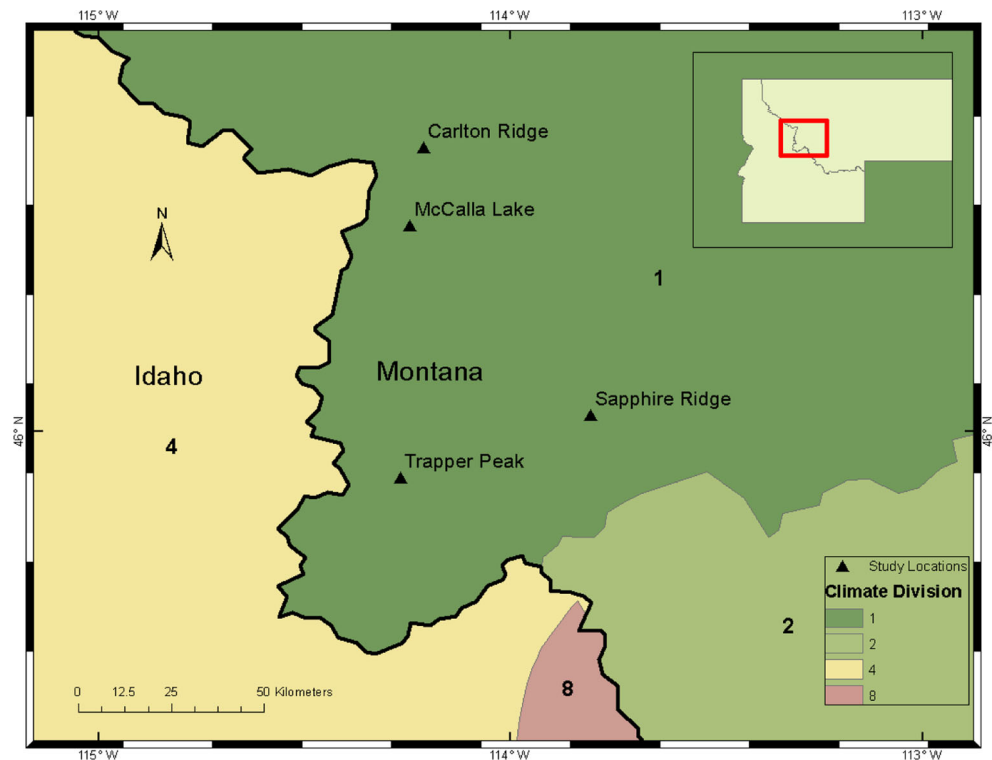
(Yamaguchi 1991). We used a high-resolution scanner to obtain digital images of each core and processed the images using the program WINDENDRO (Regent Instruments, Inc. 2011). We measured each year of each sample to 0.001 mm precision using WINDENDRO and then used the program COFECHA (Grissino-Mayer 2001; Holmes 1983) to identify and correct any errors in the dating. To maximize radial growth responses to ASIE fluctuations, we individually standardized all cores from each of the four chronologies (CRL, $n = 57$; MCL, $n = 22$; SRL $n = 28$; and TPL, $n = 42$; total $n = 149$ cores) using the program WINARSTAN (Cook 1985; <http://www.ldeo.columbia.edu/tree-ring-laboratory/resources/software>) and negative exponential curves for detrending. In prior work with the same core samples (Montpellier et al. 2018), we found negative exponential detrending best captured the climate signal.

Data, statistical analyses, and climatic reconstruction of ASIE

We obtained data on total monthly ASIE (million km²) during the satellite era (1979–current) from the National Snow and Ice Data Center (https://nsidc.org/data/seaice_index). We examined relationships between each of the 149 individual tree-ring samples and January–December monthly ASIE values during 1979–2015 using Pearson correlation and found consistent inverse relationships between ASIE and radial growth using the standardized output. The highest negative correlations occurred during January, February, and March (winter), with weakened correlations during the warmer months; thus, we selected winter for further analysis. In our analysis of individual cores, we found that temperature sensitivity varied in strength but not in direction when accounting for aspect. Specifically, we found trees growing on southerly slopes expressing the least sensitivity while trees on north and east-facing slopes were most responsive, likely due to a longer growing season during warmer summers. Ultimately, we decided to separate the trees based on aspect (cf. Montpellier et al. 2018) and created our final chronology for this study (hereafter SELECT) from trees not located on south-facing slopes and with consistently strong negative relationships ($p < 0.01$) with mean ASIE during winter (January–March). SELECT contains 44 cores (34 trees) comprised of 25 samples from Carlton Lake, five samples from McCalla Lake, and seven samples each from Sapphire Ridge and Trapper Peak. The series intercorrelation was 0.633 and mean sensitivity 0.301 spanning 1538–2015 and with an EPS of > 0.85 (Wigley et al. 1984) during 1613–2015.

We explored the possibility that regional sea-ice data may show a stronger relationship with alpine larch radial growth than ASIE data based on the entire Arctic region. Monthly regional data from 1979 to 2015 exist for five (Barents Sea; Greenland Sea; Baffin Bay; Bering Sea; East Siberian Sea) of

Fig. 1 Location of the four study sites in western Montana and boundaries of climate divisions in western Montana and eastern Idaho (created using ArcMap 10.6)



the ten regions classified by the Arctic Regional Ocean Observing system (<http://www.arctic-roos.org/observations/sea-ice-variability-in-regions>), and we compared these data with the overall ASIE data. As individual regional correlations were either non-significant or substantially lower than correlations with the overall Arctic region, we did not work with the regional data further.

We used the SELECT chronology to develop a climatic reconstruction of winter (January, February, March) mean ASIE (JFM_ASIE in million km²). Due to the short length of the satellite-era ASIE record (1979–2015 match with tree-ring data, but 1988 tree-ring or ASIE data were not included in this study as January ASIE data were missing), we verified the regression model used for the reconstruction using the leave-one-out (L1O) method (Michaelsen 1987). The verification statistics we used were the reduction in error statistic (RE), the root mean square error (RMSE), and the correlation value between the actual and predicted JFM_ASIE (Fritts 2012; Gordon 1982).

For the reconstructed JFM_ASIE, we tested for significant ($p < 0.05$) shifts in temporal regimes using the Rodionov (2004; Rodionov and Overland 2005) sequential algorithm. We detrended the 402-year reconstruction of JFM_ASIE using a moving-average set to the mean length of the temporal regimes (20 years). We used the detrended values to identify low points for JFM_ASIE in the temporal distribution. As the SELECT data were non-normally distributed based on a Shapiro–Wilk test ($p = 0.029$), we used the non-parametric Kruskal–Wallis H test to determine if there were significant

differences in the 20 years preceding the primary low points in the temporal pattern of SELECT.

To illustrate the potential suite of atmospheric linkages between JFM_ASIE and radial tree growth, we created a series of maps using the NCEP/NCAR Reanalysis dataset (Kalnay et al. 1996) and the NOAA/ESRL mapping tool (<http://www.esrl.noaa.gov/psd/>). Specifically, we examined the following: (1) June–August 1000 hPa temperature patterns in the pre- (1979–1999) and Arctic amplification eras (i.e., 2000–2015 [Francis and Vavrus 2015]); (2) 1000 hPa temperatures during the five summers with the highest and lowest reconstructed values of JFM_ASIE using the SELECT tree-ring chronology; and (3) 500 hPa anomalies during the five summers with the highest and lowest reconstructed values of JFM_ASIE using the SELECT tree-ring chronology.

We examined relationships between annual radial growth and climate using Pearson correlation between SELECT and monthly and summer (June–August) data (maximum, minimum, and mean temperature; Palmer Drought Severity Index (Palmer 1965); and precipitation) from Montana climate division 1 (<https://www.ncdc.noaa.gov/monitoring-references/maps/us-climate-divisions.php>) for the complete instrumental record (1895–2015) and for the period concurrent with satellite-derived ASIE data (1979–2015).

We tested the viability of our reconstructed JFM_ASIE values using the NOAA-ESRL twentieth century Reanalysis V2 reanalysis monthly composites during the period 1851–1978 (<https://www.esrl.noaa.gov/psd/cgi-bin/data/composites/plot20thc.v2.pl>), thus excluding the data used

(1979–2015) to create the reconstructed ASIE values. We created maps showing the North American spatial patterns of 1000 hPa June–August temperature anomalies and 500 hPa June–August geopotential height anomalies for the five highest and lowest reconstructed JFM_ASIE using the SELECT tree-ring chronology.

Results

The SELECT chronology has a significant negative relationship (r value range -0.58 to -0.73) with ASIE for all months, and the winter average (JFM_ASIE) (Table 1). For the climatic reconstruction of JFM_ASIE, the verification statistics from the L1O model were strong (RE = 0.5; RMSE = 0.36; $r = 0.71$, $p < 0.01$, between actual and predicted JFM_ASIE) and similar to those obtained for the climate reconstruction model (RE = 0.45; RMSE = 0.34; $r = 0.74$, $p < 0.01$) between actual and predicted JFM_ASIE). Residuals from the model were temporally autocorrelated, with a negative trend ($r = -0.583$, $R^2 = 0.34$, $p < 0.01$, $n = 36$) showing that the model tended to overpredict JFM_ASIE early and underpredict in later years, with the largest overprediction in 1979 of 0.76 million km² and the greatest underprediction in 2014 of 0.58 million km².

While reconstructed JFM_ASIE displays less variation than actual JFM_ASIE (coefficient of variation 2.6% and 3.5%, respectively), the reconstruction captures some of the lowest actual ASIE winters in the satellite era (1979–), with 2006 and 2015 as the two lowest ASIE years in the actual record and second and third in the reconstruction behind 2009, which had the 10th lowest actual ASIE (Fig. 2). For the 16 years in the AA era (2000–2015), eight are within the top 10% of lowest reconstructed JFM_ASIE values.

Table 1 Pearson correlations between monthly values of Arctic sea-ice extent (i.e., ASIE) and the alpine larch tree-ring chronology (i.e., SELECT) for the period 1979–2015. All relationships are significant at $p < 0.001$ and $n = 36$ (except Dec with $n = 35$). JFM is the mean of January–March ASIE

Month	r value
January	−0.724
February	−0.733
March	−0.733
April	−0.711
May	−0.713
June	−0.67
July	−0.613
August	−0.624
September	−0.582
October	−0.644
November	−0.704
December	−0.718
JFM	−0.744

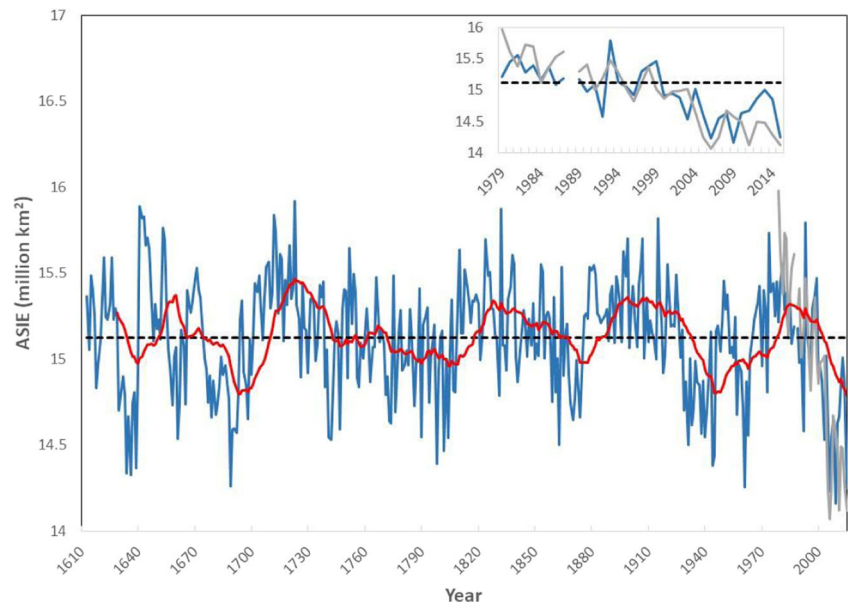
The mean length of temporal regimes was 20.1 years, and they ranged from 59 years (1809–1867) to 1 year (2015) (Fig. 3). The regime shift beginning in 2015 likely continues, as the seasonal maximum ASIE values in winters 2015 to 2018 were, respectively, the third, third (tied), first, and second lowest recorded in the satellite era (<https://nsidc.org/news/newsroom/arctic-sea-ice-maximum-second-lowest-satellite-record>).

The 20-year moving average of the tree-ring-based reconstruction of JFM_ASIE has six distinct periods where ASIE increases and then declines more slowly, with the detrended values reaching their minimum in 1640, 1693, 1805, 1874, 1946, and 2015 (Fig. 2). While the most recent cycle has the lowest reconstructed JFM_ASIE in the four-century record and this minimum was reached in the shortest time, results from the Kruskal–Wallace H test revealed that there were no significant differences ($p = 0.18$) in the six 20-year periods ending at the detrended SELECT low points.

In the northern Rocky Mountains, the AA era experienced positive surface temperature anomalies and the pre-AA (1979–1999) negative anomalies (Fig. 4a, b). In our study region (Montana Climate Division 1), the AA era was 1.1 °C warmer than the pre-AA era. Similarly, for the 5 years in the satellite era (1979–) with the lowest reconstructed winter (January–March) Arctic sea-ice extent using SELECT, the surface temperature anomalies are strongly positive, and strongly negative for the 5 years with the highest reconstructed JFM_ASIE (Fig. 5a, b). Within our study area, summer temperatures were 3.8 °C warmer when comparing the years with the five lowest and five highest reconstructed JFM_ASIE years. For the same five lowest JFM_ASIE years, the 500 hPa anomalies are strongly positive immediately upstream of the northern Rockies (Fig. 6a), suggesting enhanced ridging that leads to subsidence and the above-normal surface temperature patterns. Negative 500 hPa anomalies are found upstream of the study sites in the five highest JFM_ASIE years (Fig. 5b), suggesting troughing associated with the negative surface temperature anomalies.

When using the NOAA-ESRL twentieth-century reanalysis data, we found strongly comparable patterns for the 5 years (1851–1978) with the lowest reconstructed JFM_ASIE. Positive temperature anomalies are found throughout the Pacific Northwest and extend into our western Montana study region (Fig. 7a) in conjunction with positive 500 hPa height anomalies broadly aligned from southwest to northeast and centered upstream (i.e., northwest) of our study sites (Fig. 8a). However, unlike the satellite-area spatial patterns for the highest and lowest JMS_ASIE years (Figs. 5 and 6), there is a sharp transition zone in the western USA between anomalously high and low 1000 hPa temperatures. For the five highest reconstructed JFM_ASIE years in the pre-satellite era (1851–1978), the 1000 hPa anomalies are weakly negative over our western Montana study region, with much

Fig. 2 Reconstructed values (1613–2015) of mean wintertime (January–March) Arctic sea-ice extent (JFM_ASIE, million km²) based on a tree-ring chronology derived from alpine larch growing in western Montana (blue line). The 20-year moving average of JFM_ASIE is depicted as a red line, the actual values of Arctic sea-ice extent from 1979 to 2015 based on satellite observations are shown as a gray line, and the long-term mean value of reconstructed JFM_ASIE is shown as a dashed black line (created using Microsoft Excel)



stronger negative anomalies found in eastern Montana/North Dakota throughout much of central and western Canada (Fig. 7b). However, for 500 hPa flow, the heights are near average in western Montana and near average to marginally above normal upstream (Fig. 8), a pattern more suggestive of zonal flow in the northern Rockies.

For the full climatic record (1895–2015), we found the primary climatic driving force for radial growth of LALY to be mean maximum summer (June–August) temperature (Table 2). All relationships strengthened when using the satellite-era only data (i.e., 1979–), and the strongest

relationship was with mean summer maximum temperature (Table 2). Negative relationships with precipitation and PDSI suggest that LALY is not water-limited in this region. Further, there is a strong negative relationship ($r = -0.716$, $p < 0.01$, $n = 120$) between summer maximum temperature and summer precipitation within Montana Climate Division 1.

Discussion

Linkages between JFM_ASIE and radial tree growth of LALY are indirect and operate through thermodynamic exchanges that perturb upper-atmospheric flow patterns. Knapp and Soulé (2017) examined the relationship between January ASIE and July climatic conditions in the western USA and found significant spatial pattern correlations linking low ASIE in the prior winter to enhanced 300 hPa summer ridging upstream from the northern Rocky Mountains. In turn, this leads to positive temperature anomalies that have been shown to be the primary driving force for LALY radial growth (Kipfmüller 2008; Montpellier et al. 2018). Similarly, Montpellier (2018) found that significant positive relationships with LALY growth in western Montana are associated with 500 hPa conditions conducive to upstream summer (JJA) ridging (JJA) and significant negative relationships with 500 hPa troughing patterns. Our results for SELECT agree with these studies as radial growth is significantly and positively related to summer temperatures (Table 2).

Most pertinent to this study are studies establishing lagged linkages between AA/ASIE and perturbations in atmospheric flow. For example, Francis et al. (2009) show that summer ASIE is related to upper-atmospheric flow patterns in the

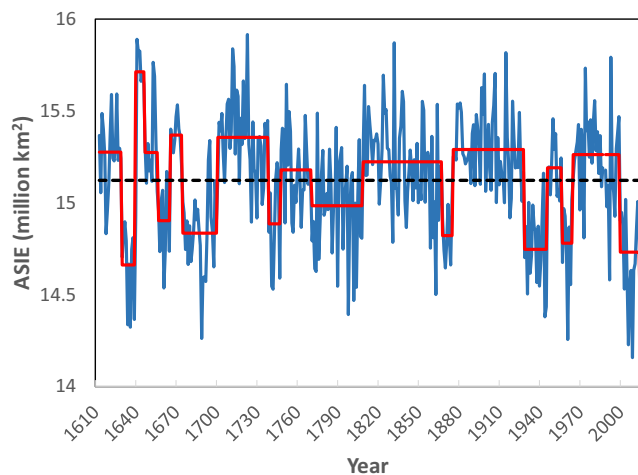
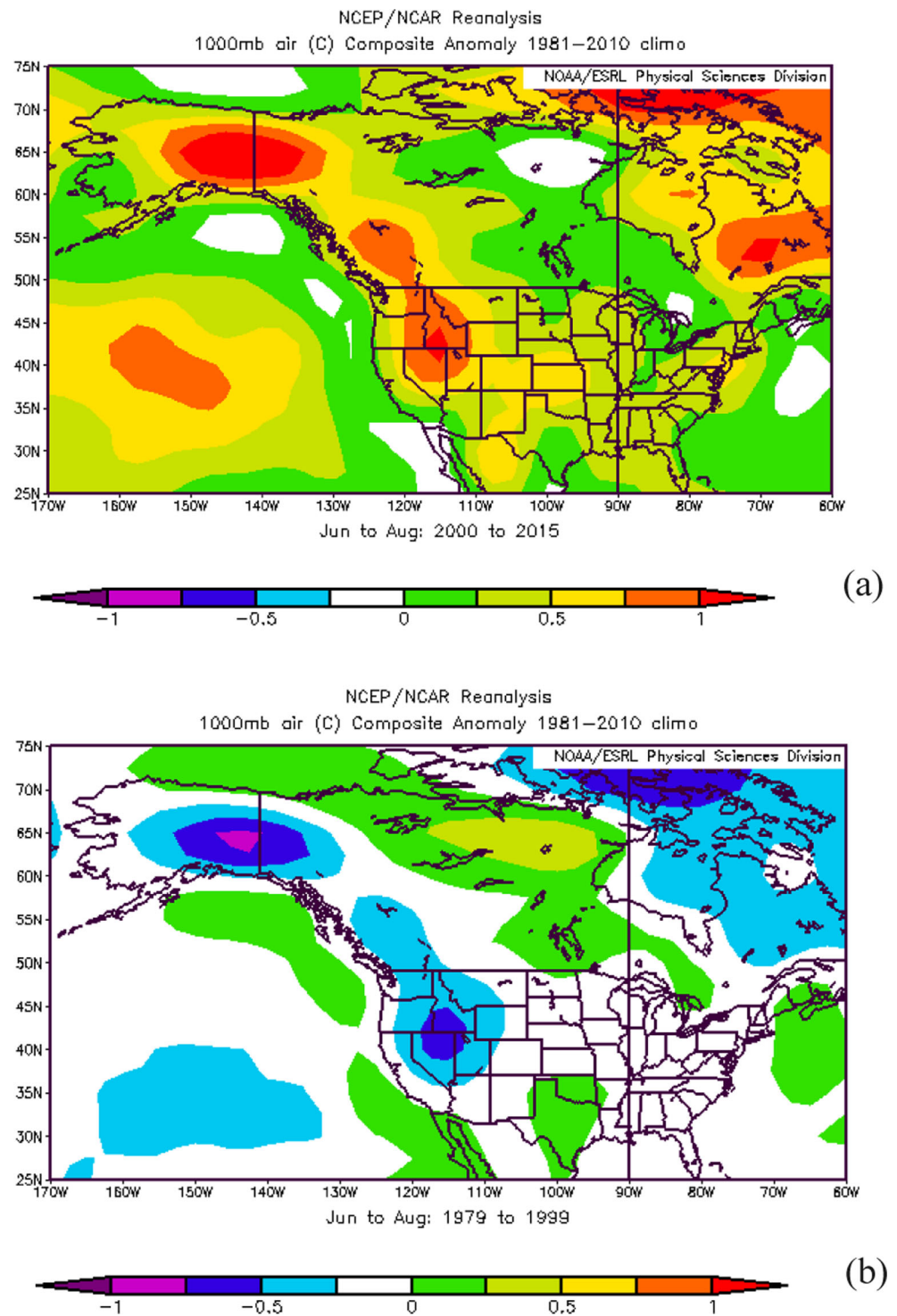


Fig. 3 Reconstructed values (1613–2015) of mean wintertime (January to March) Arctic sea-ice extent (JFM_ASIE, million km²) based on a tree-ring chronology derived from alpine larch growing in western Montana (blue line). The red line shows the mean values of JFM_ASIE during regimes and significant ($p < 0.05$) regime shifts based on the Rodionov sequential algorithm regime shift test. The dashed black line shows the long-term mean value of reconstructed JFM_ASIE (created using Microsoft Excel)

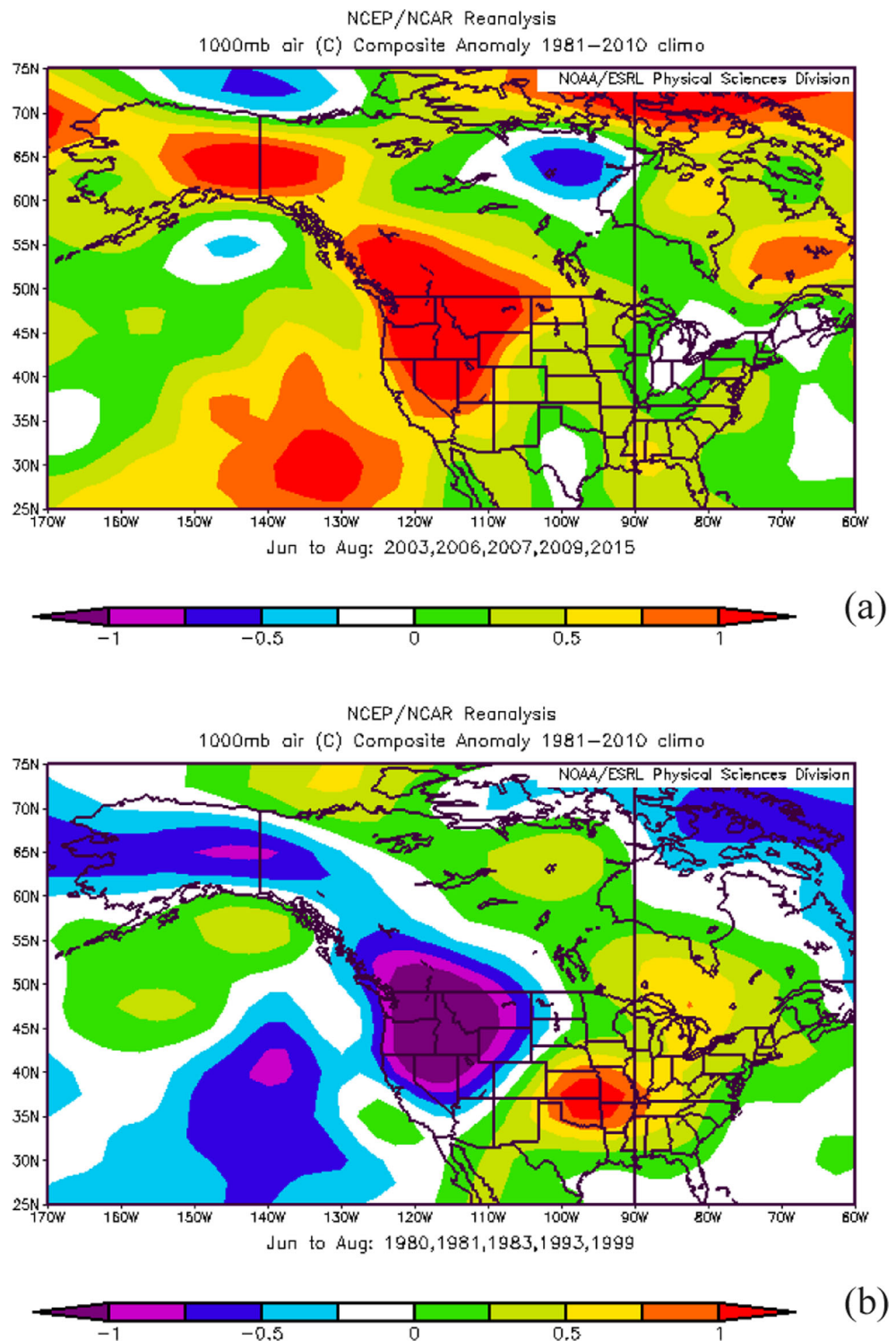
Fig. 4 **a** Anomalies of 1000 hPa temperatures (°C) for summer (June–August) during the Arctic amplification era (i.e., 2000–2015). **b** Anomalies of 1000 hPa temperatures (°C) for summer (June–August) during the earlier years of the satellite record for Arctic sea-ice extent (i.e., 1979–1999) (created using NOAA/ESRL mapping tool (<http://www.esrl.noaa.gov/psd/>))



following winter. Reduced summer ASIE is related to enhanced winter meridionality and operates through a suite of linkages including larger than normal sensible and latent heat fluxes, increased cloudiness during autumn, and modified pressure gradients (Francis et al. 2009). Lagged influences between early winter (November, December) ASIE and mid-winter (January, February) climatic perturbations were

established by Kim et al. (2014), who concluded that vertical fluxes from the troposphere ultimately lead to planetary-scale impacts from a weakened polar vortex. Both Wu et al. (2013) and Knapp and Soulé (2017) demonstrate how ASIE in the prior winter season is a driving force for climatic conditions in the following summer. The work of Wu et al. (2013) establishes a systematic linkage between regional ASIE west of

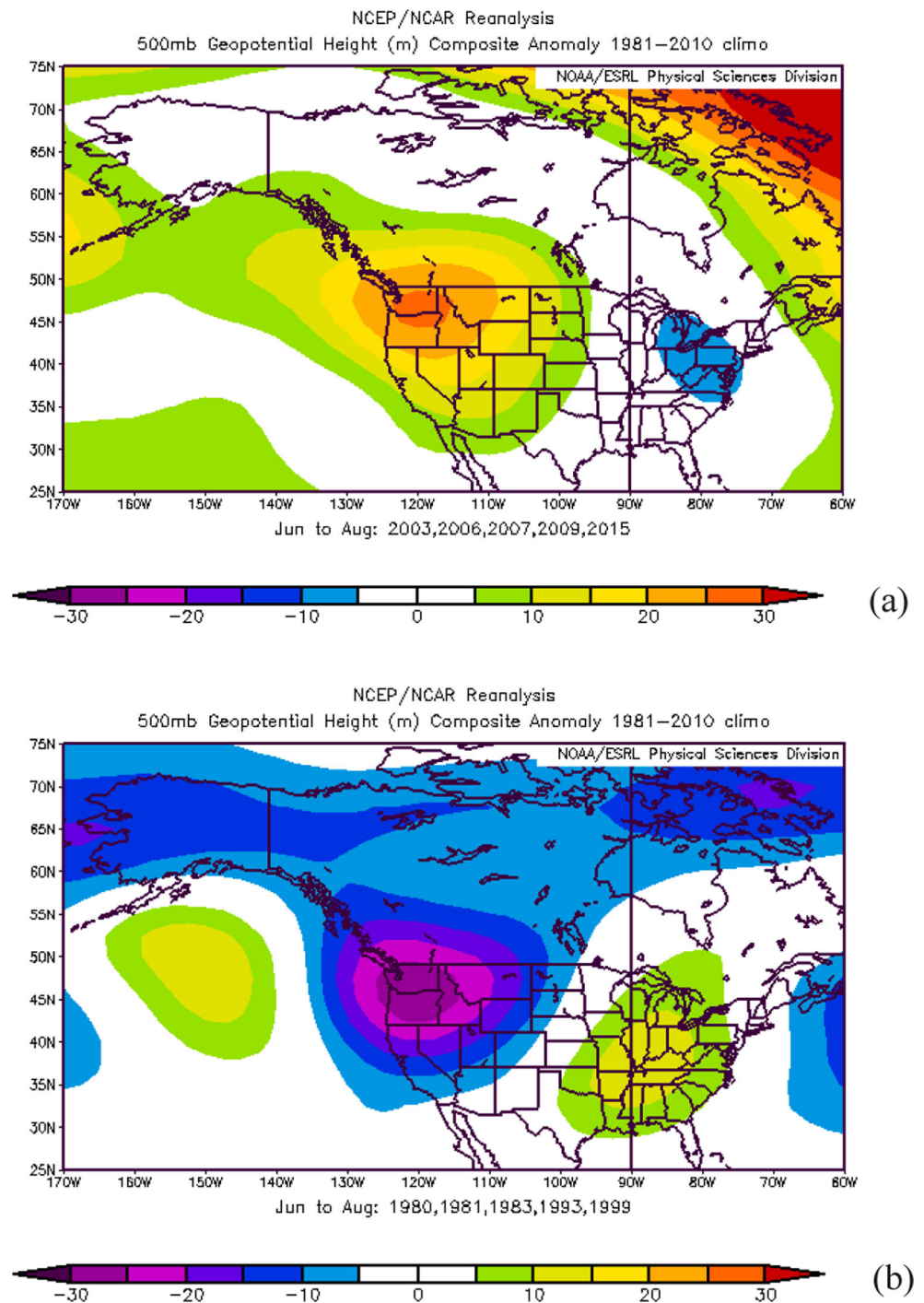
Fig. 5 a Anomalies of 1000 hPa temperatures (°C) for summer (June–August) during the 5 years with the lowest reconstructed winter (January–March) Arctic sea-ice extent using the SELECT tree-ring chronology during the instrumental era (1979–2015) for satellite observations of Arctic sea-ice extent. **b** Anomalies of 1000 hPa temperatures (°C) for summer (June–August) during the 5 years with the highest reconstructed winter (January–March) Arctic sea-ice extent using the SELECT tree-ring chronology during the instrumental era (1979–2015) for satellite observations of Arctic sea-ice extent. (created using: NOAA/ESRL mapping tool (<http://www.esrl.noaa.gov/psd/>))



Greenland and conditions in northern Eurasia whereby years of enhanced ASIE cause perturbations in North Atlantic sea surface temperatures leading to enhanced baroclinity and anomalous upper atmospheric flow patterns. Knapp and Soulé (2017) suggest a positive feedback loop where lower winter ASIE promotes ridging, leading to reductions in soil

moisture. In turn, by summer, lower soil moisture enhances surface warming leading to higher geopotential heights. Although summer moisture is significantly related to LALY growth (via either JJA precipitation or August PDSI; Table 2), we note that precipitation is a weaker driving force than temperature, particularly for LALY growing on north-facing

Fig. 6 **a** Anomalies of 500 hPa geopotential heights (m) for summer (June–August) during the 5 years with lowest reconstructed winter (January–March) Arctic sea-ice extent using the SELECT tree-ring chronology during the instrumental era (1979–2015) for satellite observations of Arctic sea-ice extent. **b** Anomalies of 500 hPa geopotential heights (m) for summer (June–August) during the 5 years with the highest reconstructed winter (January–March) Arctic sea-ice extent using the SELECT tree-ring chronology during the instrumental era (1979–2015) for satellite observations of Arctic sea-ice extent (created using NOAA/ESRL mapping tool (<http://www.esrl.noaa.gov/psd/>))

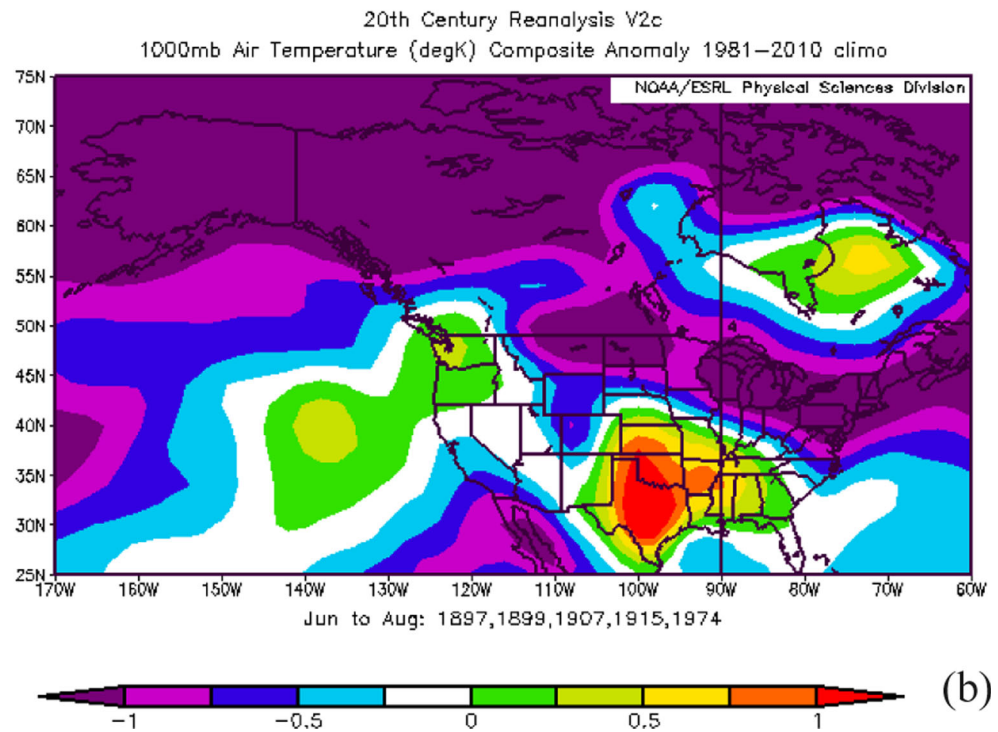
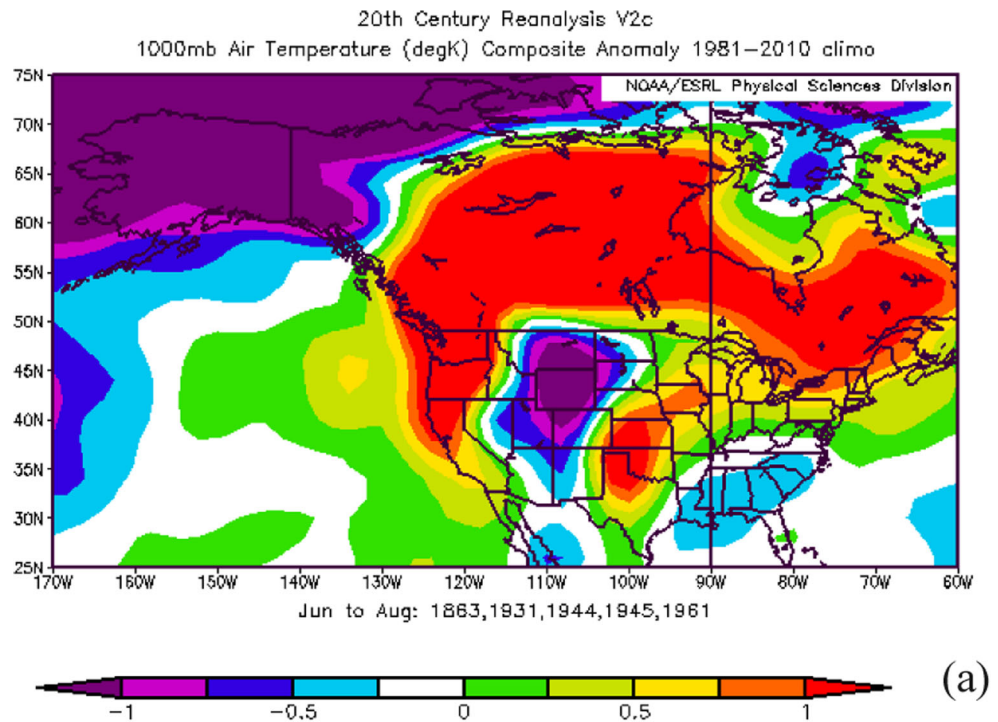


slopes (Montpellier et al. 2018). The strong inverse relationship between summer temperature (JJA) and summer precipitation supports our finding of warm (cold) years being concurrent with ridging (troughing) conditions that also produce negative (positive) precipitation anomalies.

There are likely multiple and synergistic teleconnections between ASIE and abnormal surface climatic conditions. For the western USA, Cvijanovic et al. (2017) argue for a two-step process whereby reduced ASIE initially alters the

shortwave radiation fluxes in high latitudes leading to higher heat content, which moves equatorward. In turn, this reduces tropical convective activity and upper-level divergence, leading to a “northward-propagating Rossby wavetrain with anticyclonic flow” (Cvijanovic et al. 2017, p. 6). While the focus of Cvijanovic et al. (2017) is on reduced California rainfall, the position of the enhanced ridging matches closely the patterns we found for the highest growth years for LALY (Fig. 5a).

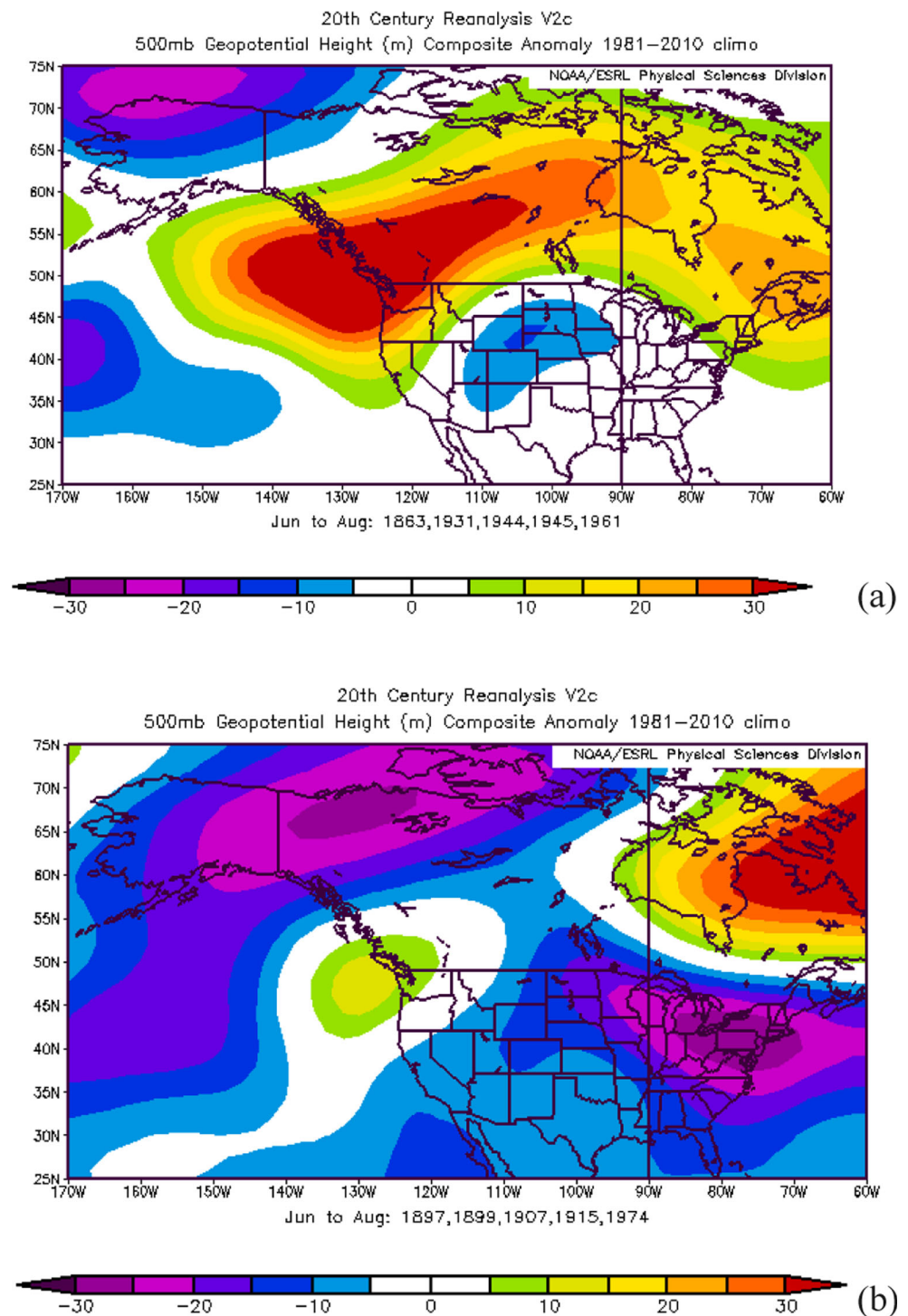
Fig. 7 a Anomalies of 1000 hPa temperatures (K) for summer (June–August) during the 5 years with the lowest reconstructed winter (January–March) Arctic sea-ice extent using the SELECT tree-ring chronology from 1851 to 1978 (beginning year of available reanalysis data through the last year when satellite measurements of ASIE were not available). **b** Anomalies of 1000 hPa temperatures (K) for summer (June–August) during the 5 years with the highest reconstructed winter (January–March) Arctic sea-ice extent using the SELECT tree-ring chronology from 1851 to 1978 (created using the NOAA-ESRL 20th century Reanalysis V2 mapping tool (<https://www.esrl.noaa.gov/psd/cgi-bin/data/composites/plot20thc.v2.pl>))



A common theme among ASIE reconstructions is that the decline of ASIE in the late twentieth to early twenty-first centuries is unmatched in the reconstructions (e.g., Halfar et al. 2013; Kinnard et al. 2011; Polyak et al. 2010; Zhang et al. 2018a). However, our results suggest that reconstructed JFM_ASIE for 1996–2015 is not significantly different from

the other five low points identified since 1613 (Fig. 2), although it contains the lowest predicted JFM_ASIE and does not include ASIE data during 2016–2018, which were also years of exceptionally low sea-ice extent. While the general cause of the recent decline is linked to anthropogenically caused warming (Stroeve et al. 2007; Kinnard et al. 2011), a

Fig. 8 **a** Anomalies of 500 hPa geopotential heights (m) for summer (June–August) during the 5 years with the lowest reconstructed winter (January–March) Arctic sea-ice extent using the SELECT tree-ring chronology from 1851 to 1978 (beginning year of available reanalysis data through the last year when satellite measurements of ASIE were not available). **b** Anomalies of 1000 hPa temperatures (K) for summer (June–August) during the 5 years with the highest reconstructed winter (January–March) Arctic sea-ice extent using the SELECT tree-ring chronology from 1851 to 1978 (created using the NOAA-ESRL 20th century Reanalysis V2 mapping tool (<https://www.esrl.noaa.gov/psd/cgi-bin/data/composites/plot20thc.v2.pl>))



broad suite of linkages between ASIE and climatic processes have been examined (e.g., Budikova et al. 2017; Francis et al. 2017; Osborne et al. 2017; Screen et al. 2015; Screen 2017; Vihma 2014). Kinnard et al. (2011) developed a 1450-year reconstruction of ASIE and compared it to reconstructed values of the North Atlantic Oscillation (NAO) and Arctic surface air temperatures. They found weak relationships, leading them to conclude that neither was the primary driving

force behind ASIE fluctuations. We also compared our reconstructed JFM_ASIE values to a reconstructed NAO index (Luterbacher et al. 2001) from the period AD 1659–2001 and found weak ($r < 0.096$) and non-significant relationships ($p > 0.05$) for both annual and monthly (January, February, March) comparisons. However, when we compared our reconstructed JFM_ASIE values to measurements of surface oceanic temperature anomalies (60–90° N) from AD 1880–

Table 2 The strongest correlations between the alpine larch tree-ring chronology (i.e., SELECT) and the following climatic parameters obtained from Montana Climatic Division 1 for the periods 1895–2015 ($n = 120$) and 1979–2015 ($n = 36$): June, July, August, and summer mean (July–August; JJA) temperature; June, July, August, and summer mean maximum temperature; June, July, August, and summer mean minimum temperature; June, July, August, and summer mean precipitation; June, July, August, and summer mean values of the Palmer Drought Severity Index (PDSI)

Variable	Correlation (* $p < 0.01$; ** $p < 0.001$) 1895–2015
Mean temperature (JJA)	0.514**
Maximum temperature (JJA)	0.528**
Minimum temperature (JJA)	0.225**
Precipitation (JJA)	−0.374**
PDSI (August)	−0.443**
Variable	Correlation (* $p < 0.01$; ** $p < 0.001$) 1979–2015
Mean temperature (JJA)	0.577**
Maximum temperature (JJA)	0.575**
Minimum temperature (JJA)	0.473*
Precipitation (JJA)	−0.471*
PDSI (August)	−0.545*

2015 (Zhang et al. 2018b), we found significant ($p < 0.001$) negative relationships with both annual ($r = -0.584$) and seasonal (January–March) values ($r = -0.527$), suggesting a logical connection between increasing high-latitude oceanic temperature and decreasing ASIE.

We recognize potential caveats to our findings. First, the analysis period to develop reconstructed ASIE values was based on the 35-year satellite era of 1979–2015 (end of our tree-ring data and excluding 1988); thus, we recognize the potential volatility of our results. However, our comparison of the top-five lowest reconstructed JFM_ASIE years pre-1979 with 1000 hPa temperature and 500 hPa height anomalies (Fig. 7) produced spatial patterns largely consistent with those found during the satellite era (Figs. 4, 5, and 6). Specifically, years of low wintertime sea-ice extent are associated with enhanced upper-level ridging in the Pacific Northwest and positive surface temperature anomalies throughout the Pacific Northwest and northern Rockies. Spatial patterns of 1000 hPa temperature anomalies and 500 hPa geopotential height anomalies for the five highest reconstructed JFM_ASIE years prior to the satellite era (1851–1978) (Figs. 7 and 8) are not as strongly in-phase with patterns from the satellite era (1979–2015; Figs. 5 and 6), potentially suggesting a stronger teleconnection between wintertime ASIE and summer weather conditions in the western USA during periods of low sea-ice extent. Overall, our results

suggest that our reconstructed JFM_ASIE values capture key elements of the interannual variability shown during the calibration period, and in the absence of a longer historical measurements of sea-ice extent, serve as a validation of the reconstruction. Second, our analyses are based on data capturing only the historic temporal variability of sea-ice extent and not the cause(s) for Arctic amplification. Francis (2017) notes that multiple factors have been identified as causes of Arctic amplification (e.g., sea-ice thinning, declining Northern Hemisphere snow cover), and these synergistic interactions contribute to various positive-feedback mechanisms potentially driving sea-ice loss. Thus, the linkages between our observations of a connection between winter sea-ice extent and atmospheric processes over western North America in summer as captured by tree-ring width variability unlikely accounts for the full complexity of this relationship.

Conclusions

Our results suggest that considerable variability in ASIE has occurred during the past four centuries and may have a strong climatological influence on regions far removed from the Arctic. In the instrumental era spanned by our study (1979–2015), wintertime ASIE has decreased by 1.9 million km², an area equivalent in size to Mexico, yet absent the use of proxy data the magnitude of this change is poorly understood in a historical context. Our reconstructed values of JFM_ASIE suggest that the current decline is preceded relative to five other low-ASIE periods in the last 400+ years, but the driving forces behind the recent contraction are likely related to unprecedented anthropogenically driven changes (e.g., CO₂ levels exceeding 400 ppmv) in our atmospheric system (Kinnard et al. 2011; Stroeve et al. 2007) that should continue in the upcoming decades. Further, if ASIE continues trending downward as has occurred post-2015 (e.g., actual JFM_ASIE in 2016, 2017, and 2018 rank as the 5th, 2nd, and 1st lowest during the satellite-recording era of 1979–2018), the most recent period will become unmatched in the context of the past four centuries. Tree-ring-based reconstructions of any climatic or environmental variable are limited by the inherent multiple driving forces affecting tree growth. Yet, the linkages identified herein are unique in that they suggest a geographically remote species can be influenced by environmental conditions occurring in the Arctic through a broad suite of atmospheric teleconnections associated with this decline. Thus, this long-lived tree species in the northern Rocky Mountains is both affected by changes in ASIE and serves as a useful biological recorder of environmental change.

Acknowledgments We thank Tyler Mitchell for the production of Fig. 1. We thank Steve Shelly, Justin Maxwell, and Evan Montpellier for their assistance during fieldwork.

Support for the Twentieth Century Reanalysis Project dataset is provided by the U.S. Department of Energy, Office of Science Innovative and Novel Computational Impact on Theory and Experiment (DOE INCITE) program, and Office of Biological and Environmental Research (BER), and by the National Oceanic and Atmospheric Administration Climate Program Office.

Funding We thank Appalachian State University and the University of North Carolina-Greensboro for internal funding that made the collection of tree-ring samples possible.

References

- Amo SF, Habeck JR (1972) Ecology of alpine larch (*Larix lyallii* Parl.) in the Pacific Northwest. *Ecol Monogr* 42(4):417–450
- Budikova D, Chechi L (2016) Arctic sea ice and warm season North American extreme surface air temperatures. *Clim Res* 67(1):15–29
- Budikova D, Ford TW, Ballinger TJ (2017) Connections between north-central United States summer hydroclimatology and Arctic sea ice variability. *Int J Climatol* 37(12):4434–4450
- Cattiaux J, Peings Y, Saint-Martin D, Trou-Kechout N, Vavrus SJ (2016) Sinuosity of midlatitude atmospheric flow in a warming world. *Geophys Res Lett* 43(15):8259–8268
- Cohen J, Screen JA, Furtado JC, Barlow M, Whittleston D, Coumou D, Francis J, Dethloff K, Entekhabi D, Overland J, Jones J (2014) Recent Arctic amplification and extreme mid-latitude weather. *Nat Geosci* 7(9):627–637
- Cook ER (1985) A time series analysis approach to tree ring standardization. Master's thesis, University of Arizona
- Cvijanovic I, Santer BD, Bonfils C, Lucas DD, Chiang JC, Zimmerman S (2017) Future loss of Arctic sea-ice cover could drive a substantial decrease in California's rainfall. *Nat Commun* 8(1):1947
- Fauria MM, Grinsted A, Helama S, Moore J, Timonen M, Martma T et al (2010) Unprecedented low twentieth century winter sea ice extent in the Western Nordic seas since AD 1200. *Clim Dyn* 34(6):781–795
- Francis JA (2017) Why are Arctic linkages to extreme weather still up in the air? *Bull Am Meteorol Soc* 98(12):2551–2557
- Francis JA, Vavrus SJ (2015) Evidence for a wavier jet stream in response to rapid Arctic warming. *Environ Res Lett* 10(1):014005
- Francis JA, Chan W, Leathers DJ, Miller JR, Veron DE (2009) Winter Northern Hemisphere weather patterns remember summer Arctic sea-ice extent. *Geophys Res Lett* 36(7)
- Francis JA, Vavrus SJ, Cohen J (2017) Amplified Arctic warming and mid-latitude weather: new perspectives on emerging connections. *Wiley Interdiscip Rev Clim Chang* 8(5):e474
- Fritts HC (2012) *Tree rings and climate*. Elsevier, Amsterdam
- Gordon GA (1982) Verification of dendroclimatic reconstructions. In: Hughes MK et al (eds) *Climate from tree rings*. Cambridge University Press, Cambridge, U.K., pp 58–61
- Graumlich LJ, Brubaker LB (1986) Reconstruction of annual temperature (1590–1979) for Longmire, Washington, derived from tree rings. *Quat Res* 25(2):223–234
- Grissino-Mayer HD (2001) Evaluating crossdating accuracy: a manual and tutorial for the computer program COFECHA. *Tree-ring research* 57:205–221
- Halfar J, Adey WH, Kronz A, Hetzinger S, Edinger E, Fitzhugh WW (2013) Arctic sea-ice decline archived by multicentury annual-resolution record from crustose coralline algal proxy. *Proc Natl Acad Sci* 110(49):19737–19741
- Hall RJ, Jones JM, Hanna E, Scaife AA, Erdélyi R (2017) Drivers and potential predictability of summer time North Atlantic polar front jet variability. *Clim Dyn* 48(11–12):3869–3887
- Holmes RL (1983) Computer-assisted quality control in tree-ring dating and measurement. *Tree-Ring Bull*
- Kalnay E, Kanamitsu M, Kistler R, Collins W, Deaven D, Gandin L et al (1996) The NCEP/NCAR 40-year reanalysis project. *Bull Am Meteorol Soc* 77(3):437–471
- Kim BM, Son SW, Min SK, Jeong JH, Kim SJ, Zhang X, Shim T, Yoon JH (2014) Weakening of the stratospheric polar vortex by Arctic sea-ice loss. *Nat Commun* 5:4646
- Kinnard C, Zdanowicz CM, Fisher DA, Isaksson E, de Vernal A, Thompson LG (2011) Reconstructed changes in Arctic sea ice over the past 1,450 years. *Nature* 479(7374):509–512
- Kipfmueller KF (2008) Reconstructed summer temperature in the northern Rocky Mountains wilderness, USA. *Quat Res* 70(2):173–187
- Knapp PA, Soulé PT (2011) Reconstructing annual area burned in the northern Rockies, USA: AD 1626–2008. *Geophys Res Lett* 38(17):L17402. <https://doi.org/10.1029/2011G1048119>
- Knapp PA, Soulé PT (2017) Spatio-temporal linkages between declining Arctic sea-ice extent and increasing wildfire activity in the western United States. *Forests* 8(9):313–325
- Luterbacher J, Xoplaki E, Dietrich D, Jones PD, Davies TD, Portis D et al (2001) Extending North Atlantic oscillation reconstructions back to 1500. *Atmos Sci Lett* 2(1–4):114–124
- Mann ME, Rahmstorf S, Kornhuber K, Steinman BA, Miller SK, Coumou D (2017) Influence of anthropogenic climate change on planetary wave resonance and extreme weather events. *Sci Rep* 7:45242
- Méheust M, Stein R, Fahl K, Max L, Riethdorf JR (2016) High-resolution IP 25-based reconstruction of sea-ice variability in the western North Pacific and Bering Sea during the past 18,000 years. *Geo-Mar Lett* 36(2):101–111
- Michaelsen J (1987) Cross-validation in statistical climate forecast models. *J Clim Appl Meteorol* 26(11):1589–1600
- Montpellier EE (2018) Reconstructing summer upper-level flow in the northern Rocky Mountains using an alpine larch (*Larix lyallii*) tree-ring chronology. Master's Thesis. Appalachian State University, Boone, NC
- Montpellier EE, Soulé PT, Knapp PA, Shelly JS (2018) Divergent growth rates of alpine larch trees (*Larix lyallii* Parl.) in response to micro-environmental variability. *Arct Antarct Alp Res* 50(1):e1415626
- Osborne JM, Screen JA, Collins M (2017) Ocean–atmosphere state dependence of the atmospheric response to Arctic sea ice loss. *J Clim* 30(5):1537–1552
- Overland J, Francis JA, Hall R, Hanna E, Kim SJ, Vihma T (2015) The melting Arctic and midlatitude weather patterns: are they connected. *J Clim* 28(20):7917–7932
- Palmer WC (1965) *Meteorological drought*, vol 30. US Department of Commerce, Weather Bureau, Washington, DC
- Polyak L, Alley RB, Andrews JT, Brigham-Grette J, Cronin TM, Darby DA et al (2010) History of sea ice in the Arctic. *Quat Sci Rev* 29(15–16):1757–1778
- Regent Instruments Canada Inc (2011) WINDENDRO for tree-ring analysis. Canada Inc, Québec, Canada
- Rodionov SN (2004) A sequential algorithm for testing climate regime shifts. *Geophys Res Lett* 31(9):L09204. <https://doi.org/10.1029/2004GL019448>
- Rodionov S, Overland JE (2005) Application of a sequential regime shift detection method to the Bering Sea ecosystem. *ICES J Mar Sci* 62(3):328–332
- Screen JA (2013) Influence of Arctic sea ice on European summer precipitation. *Environ Res Lett* 8(4):044015
- Screen JA (2017) The missing Northern European winter cooling response to Arctic sea ice loss. *Nat Commun* 8:14603

- Screen JA, Deser C, Sun L (2015) Reduced risk of North American cold extremes due to continued Arctic sea ice loss. *Bull Am Meteorol Soc* 96(9):1489–1503
- Spolaor A, Vallelonga P, Turetta C, Maffezzoli N, Cozzi G, Gabrieli J, Barbante C, Goto-Azuma K, Saiz-Lopez A, Cuevas CA, Dahl-Jensen D (2016) Canadian Arctic sea ice reconstructed from bromine in the Greenland NEEM ice core. *Sci Rep* 6:33925
- Stokes MA (1996) An introduction to tree-ring dating. University of Arizona Press, Tucson
- Stroeve J, Holland MM, Meier W, Scambos T, Serreze M (2007) Arctic sea ice decline: faster than forecast. *Geophys Res Lett* 34(9): L09501. <https://doi.org/10.1029/2007GL029703>
- Tang Q, Zhang X, Yang X, Francis JA (2013) Cold winter extremes in northern continents linked to Arctic sea ice loss. *Environ Res Lett* 8(1):014036
- Tang Q, Zhang X, Francis JA (2014) Extreme summer weather in northern mid-latitudes linked to a vanishing cryosphere. *Nat Clim Chang* 4(1):45–50
- Trouet V, Babst F, Meko M (2018) Recent enhanced high-summer North Atlantic Jet variability emerges from three-century context. *Nat Commun* 9(1):180
- Vavrus SJ, Wang F, Martin JE, Francis JA, Peings Y, Cattiaux J (2017) Changes in North American atmospheric circulation and extreme weather: influence of Arctic amplification and Northern Hemisphere snow cover. *J Clim* 30(11):4317–4333
- Vihma T (2014) Effects of Arctic sea ice decline on weather and climate: a review. *Surv Geophys* 35(5):1175–1214
- Walsh JE, Fetterer F, Scott Stewart J, Chapman WL (2017) A database for depicting Arctic sea ice variations back to 1850. *Geogr Rev* 107(1): 89–107
- Wigley TM, Briffa KR, Jones PD (1984) On the average value of correlated time series, with applications in dendroclimatology and hydro-meteorology. *J Clim Appl Meteorol* 23(2):201–213
- Wu B, Zhang R, D'Arrigo R, Su J (2013) On the relationship between winter sea ice and summer atmospheric circulation over Eurasia. *J Clim* 26(15):5523–5536
- Yamaguchi DK (1991) A simple method for cross-dating increment cores from living trees. *Can J For Res* 21(3):414–416
- Zhang Q, Xiao C, Ding M, Dou T (2018a) Reconstruction of autumn sea ice extent changes since 1289 AD in the Barents-Kara Sea, Arctic. *Sci Sin Terrae* 61:1279–1291. <https://doi.org/10.1007/s11430-017-9196-4>
- Zhang HM, Huang B, Lawrimore J, Menne M, Smith TM (2018b) NOAA Global Surface Temperature Dataset (NOAAGlobalTemp), Version 4.0. NOAA National Centers for Environmental Information. <https://doi.org/10.7289/V5FN144H>. Accessed June 1 2018